Vietnam Journal of Mechanics, Vol. 45, No. 4 (2023), pp. 334 – 357
DOI: https://doi.org/10.15625/0866-7136/19613

PROPORTIONAL TOPOLOGY OPTIMIZATION ALGORITHM WITH VIRTUAL ELEMENTS FOR MULTI-MATERIAL PROBLEMS CONSIDERING MASS AND COST CONSTRAINTS

Minh Tuan Tran[1,*], **Minh Ngoc Nguyen**[2,3,**]
[1]*Department of Mechanical Engineering, Vietnamese German University, Ring road 4, Quarter 4, Thoi Hoa Ward, Ben Cat Town, Binh Duong Province, Vietnam*
[2]*Duy Tan Research Institute for Computational Engineering (DTRICE), Duy Tan University, Ho Chi Minh city 700000, Vietnam*
[3]*Faculty of Civil Engineering, Duy Tan University, Da Nang 550000, Vietnam*
[*]E-mail: minh.tt@vgu.edu.vn
[**]E-mail: nguyenngocminh6@duytan.edu.vn

Received: 08 December 2023 / Revised: 28 December 2023 / Accepted: 30 December 2023
Published online: 31 December 2023

Abstract. This paper presents an extension of the Proportional Topology Optimization (PTO) with virtual elements for multi-material problems with mass and cost constraints. In particular, the linear virtual element method (VEM) is constructed on unstructured polygonal meshes. The linear VEM is desirable in the sense that numerical integration is not explicitly required, significantly reducing the computational effort. Furthermore, the unstructured polygonal mesh naturally eliminates the issue of one-node connections encountered by the usual quadrilateral mesh. A feature of PTO is that it does not require sensitivity information, i.e., the derivative of the objective function with respect to design variables. Instead, the amount of material distributed into each element is determined proportionally to the contribution of that element to the objective function. For multi-material problems, the Ordered Solid Isotropic Material with Penalization (Ordered SIMP) technique is integrated into the PTO framework. Compared to other techniques for problems that involve multiple materials, Ordered SIMP has the advantage that computational cost does not depend on the number of materials. Furthermore, for the first time, the PTO approach is extended to consider two types of constraints: mass and cost simultaneously. The feasibility and efficiency of the proposed method are demonstrated via several benchmark examples and comparisons with the existing approach.

Keywords: linear virtual element method, proportional topology optimization, ordered SIMP, multi-material.

1. INTRODUCTION

Topology optimization aims to seek the material layout leading to the best structural performance under specified loading and boundary conditions. Since the pioneering works by [1, 2], the approach has progressively emerged as a useful numerical tool for engineers in the early stage of designing products. A large number of contributions have been made by many authors, which can be classified into different groups of methods, including the density-based approach [2–4], level set approach [5–7], phase field approach [8,9], and explicit methods [10–13]. In practice, multi-material designs are usually needed, for e.g., in order to reduce mass and/or cost. The extension of the density-based approach using the Solid Isotropic Material with Pe-nalization (SIMP) or the Rational Approximation of Material Properties (RAMP) to take multiple materials into account was discussed by [14, 15]. Employment of multiple level set functions was proposed by [16, 17], in which each material phase is represented by a different combination of the level set functions. The phase field model for multi-material topology optimization was developed based on generalized Cahn-Hilliard equations [18]. Tavakoli and Mohseni [19] introduced the so-called Alternating Active Phase Algorithm (AAPA), in which a multi-material problem is divided into a series of two-phase sub-problems. As a single-material problem can be regarded as a two-phase problem, this idea enables a relatively straightforward extension of many existing approaches to consider multiple materials. Therefore, AAPA has been employed by many authors for the investigation of various problem types [20–26]. The main drawback of AAPA is that computational effort quickly scales up with respect to the number of materials. Alternatively, the Ordered SIMP scheme was proposed by Zuo and Saitou [27] with an interesting feature that computational cost does not depend on the number of materials. Since the introduction, the Ordered SIMP has been further explored for stress-constrained problems [28] and multi-scale problems [29]. A modified interpolation scheme together with a threshold projection being tailored for Ordered SIMP was discussed by [30].

The majority of works available in literature require sensitivity information, i.e., the derivative of the objective function with respect to design variables. On the other hand, there exist alternative methods in which design variables are updated mainly by the objective values. Early attempts at such methods rely on meta-heuristic search algorithms such as modified binary Differential Evolution [31], Genetic algorithm [32], Particle Swarm Optimization [33], etc. However, they were criticized by [34] for inefficiency. Although the meta-heuristic algorithms aim to conduct the global search, there is no guarantee for the global optimum. Furthermore, the computational cost may quickly scale up with the number of design variables. Recently, some new other techniques have been developed, for e.g., the combination of the level set method with pattern search [35, 36], the combination of Material-field series-expansion with the Kriging

algorithm [37], and the cellular automata [38–40]. A density-based approach, namely Proportional Topology Optimization, was proposed by Biyikli and To [41] for problems of finding minimum structural compliance. In this approach, material distribution into each element is proportional to the contribution of that element to the total value of the objective function. Later, an improved PTO version was discussed [42]. The effect of load uncertainty was integrated into the PTO procedure by [43]. The capability of the method in mass minimization with the constraint on stress was explored by [41, 43, 44]. Extension of PTO for multi-material topology optimization with the aid of a modified SIMP scheme [45] or AAPA [22] were also investigated. However, so far, there is still no work on PTO that considers both mass and cost constraints. In fact, the number of works on methods for topology optimization without calculation of sensitivity is still very limited. The number of studies on such methods for multi-material problems is even less.

Although the Finite Element Method (FEM) is currently the most popular tool for solving equilibrium equations, the application of FEM with usual triangular or quadrilateral elements into topology optimization may encounter the one-node connection issue [46]. On the other hand, in an unstructured polygonal mesh, two adjacent elements share one edge connecting two common vertices. Hence, the issue of one-node connections is eliminated—however, computational cost increases when polygonal elements are employed. In the last decade, da Veiga et al. introduced the Virtual Element Method (VEM) [47,48] for numerical analysis in domains discretized by a general polytope mesh. The interesting idea of VEM is that there is no explicit shape function. Instead, a set of projection operators are constructed to project the shape functions of each element and their derivatives onto a space of polynomials up to a given degree k. These projections can be computed using the field degrees of freedom (DOFs). Therefore, by some mathematical transformation, the stiffness matrix can be calculated without numerical integration, at least in linear elasticity [49]. Furthermore, the VEM is less sensitive to distorted elements, e.g., those containing a high aspect ratio or too acute/obtuse angle. Details on the implementation of VEM can be found in the available kinds of literature, e.g., see [50, 51]. Since the introduction, VEM has been increasingly gaining popularity. The capability of the method has been explored and demonstrated by various authors for the analysis of finite deformation [52], material inelasticity [53], contact problems [54], fracture mechanics [55] and topology optimization [49, 56, 57].

In this paper, the Ordered SIMP technique is incorporated into the PTO algorithm for multi-material problems. It is expected to utilize the low-computational cost advantage of Ordered SIMP. In previously published works [22, 45], the constraint on the volume fraction of material phases was considered. Here, for the first time, the PTO algorithm is extended to consider constraints on both material mass and material cost simultaneously. The efficiency of the proposed method is investigated via comparison with the available

approach introduced in [30]. For discretization of the problem domain, unstructured polygonal meshes could be obtained by the available tool PolyMesher [58]. Fast computation of the element stiffness matrix is conducted using VEM. The paper is organized as follows. After the Introduction is a brief description on Virtual Element Method in Section 2. Section 3 is reserved for the proposed multi-material Proportional Topology Optimization with the Ordered SIMP algorithm. Numerical results are presented in Section 4. Finally, some concluding remarks are given in Section 5.

2. VIRTUAL ELEMENT METHOD

The linear VEM framework in this section followed the concept of Ortiz-Bernardin et al. [51] and Gain et al. [50]. VEM does not require the computation of the interpolation functions in the interior of the elements. The critical concept is the computation of elemental strain energy that is exact for the linear deformations without volumetric integration of the basis functions. What facilitates this calculation is the projection operators that separate the element deformation into its polynomial and non-polynomial components. More significantly, in linear VEM formulation, two projection maps linked with rigid body motion and constant strain deformations are employed to decompose this kinematic relation.

2.1. Model description and discretization

Consider an elastic solid, in undeformed configuration, that occupies a domain $\Omega \in R^2$ with $\partial\Omega$ being its boundary whose unit outward normal is $\mathbf{n}$. The solid body is now subjected to body forces $\mathbf{b}$ in Ω, a prescribed displacement field u^* on Γ_u (Dirichlet boundary), and prescribed external traction $\mathbf{t}^*$ on Γ_t (Neumann boundary), so that $\Gamma_u \cup \Gamma_t = \partial\Omega$ and $\Gamma_u \cap \Gamma_t = \infty$. The Galerkin variational form of this problem is stated as follows: Find the displacement field $u \in V$ such that

$$a(\mathbf{u}, \mathbf{v}) = L(\mathbf{v}), \quad \forall \mathbf{v} \in \mathcal{V}_0, \tag{1}$$

where

$$a(\mathbf{u}, \mathbf{v}) = \int_\Omega [\mathbf{C}\boldsymbol{\varepsilon}(\mathbf{u})] : \boldsymbol{\varepsilon}(\mathbf{v}) \mathrm{d}x, \qquad L(v) = \int_\Omega \mathbf{b} \cdot \mathbf{v} \mathrm{d}\Omega + \int_{\Gamma_t} \mathbf{t}^* \cdot \mathbf{v} \mathrm{d}\Gamma, \tag{2}$$

are respectively the energy bilinear form and load linear form. In Eq. (2), $\mathbf{C}$ is the elasticity tensor, and the strain field $\boldsymbol{\varepsilon}(\boldsymbol{u}) = \frac{1}{2}(\nabla\mathbf{u} + \nabla\mathbf{u}^T)$ is defined as a linearized strain tensor. Moreover, the displacement trial space V and the space of admissible displacement field $\mathcal{V}_0$ belonging to first order Sobolev space $\mathcal{H}^1(\Omega)$ as in the following

$$\mathcal{V} = \left\{ \mathbf{u}(\mathbf{x}) : \mathbf{u} \in \mathcal{L}(\Omega) \subseteq [\mathcal{H}^1(\Omega)]^2, \quad \mathbf{u} = \mathbf{u}^* \text{ on } \quad \Gamma_u \right\}, \tag{3}$$

$$\mathcal{V}_0 = \left\{ \mathbf{v}(\mathbf{x}) : \mathbf{v} \in \mathcal{L}(\Omega) \subseteq [\mathcal{H}^1(\Omega)]^2, \quad \mathbf{v} = \mathbf{0} \text{ on } \quad \Gamma_u \right\}, \tag{4}$$

where $\mathcal{L}(\Omega)$ includes linear displacement field.

For approximated Galerkin solution, let us consider a partitioned domain $\Omega^h \approx \Omega$ consisting of arbitrarily non-overlapping polygonal regions. This partition Ω^h is well-known as a mesh with h being the maximum diameter of an arbitrary element E, which does not need to be convex and can have any arbitrary shape with different node numbers. With the aid of basis functions, the continuous trial and test displacement fields u and v are approximated by the discrete vector fields $\mathbf{u}^h$ and $\mathbf{v}^h$ belongs to discrete global trial and test spaces such that the bilinear and linear form in Eq. (2) can be respectively represented as a summation of elemental contributions in the mesh, as follows

$$a(\mathbf{u},\mathbf{v}) \approx a(\mathbf{u}^h,\mathbf{v}^h) = \sum_{E\in\Omega^h} a_E(\mathbf{u}^h,\mathbf{v}^h), \tag{5}$$

$$a_E(\mathbf{u}^h,\mathbf{v}^h) = \int_E [\mathbf{C}\boldsymbol{\varepsilon}(\mathbf{u}^h)] : \boldsymbol{\varepsilon}(\mathbf{v}^h) dx, \tag{6}$$

and

$$L(\mathbf{v}) \approx L(\mathbf{v}^h) = \sum_{E\in\Omega^h} L_{b,E}(\mathbf{v}^h) + \sum_{e\in\Gamma_t^h} L_{t,E}(\mathbf{v}^h), \tag{7}$$

$$L_{b,E}(\mathbf{v}^h) = \int_E \mathbf{b}\cdot\mathbf{v}^h d\Omega \qquad L_{b,E}(\mathbf{v}^h) = \int_e \mathbf{t}^*\cdot\mathbf{v}^h d\Gamma. \tag{8}$$

It is worth noting here the definition of discrete global trial and test spaces as follows

$$\mathcal{V}^h = \left\{ \mathbf{u}^h(\mathbf{x}) \in \mathcal{V} : \mathbf{u}^h|_E \in \mathcal{L}(E)) \subseteq [\mathcal{H}^1(\Omega)]^2, \quad \forall E \in \Omega^h \right\}, \tag{9}$$

$$\mathcal{V}_0^h = \left\{ \mathbf{v}^h(\mathbf{x}) \in \mathcal{V}_0 : \mathbf{v}^h|_E \in \mathcal{L}(E)) \subseteq [\mathcal{H}^1(\Omega)]^2, \quad \forall E \in \Omega^h \right\}, \tag{10}$$

where $\mathcal{L}(E)$ is the element space containing all the deformation states, i.e., linear deformations and higher-order modes, represented by the element E. We will see later that VEM only concerns the behaviour of functions in $\mathcal{L}(E)$ on the boundary, not in the interior of E.

In general, due to the arbitrary-shaped elements E, the basis functions are not necessarily polynomial functions. Therefore, these weak-form integrals are evaluated using the quadrature rule (see Eqs. (5) and (7)) with a high possibility of generating numerical integration errors that typically lead to mesh-dependent problems directly affecting the convergence of the numerical solution. Even using a prohibitively large number of integration points in each element to guarantee convergence is not a helpful answer due to its high computational cost. The situation is entirely different in the VEM approach: the terms in Eqs. (5) and (7) can be evaluated without the requirement of numerical integration, such as Gauss's points scheme. Alternatively, these elemental bilinear and linear forms only need a *projection operator* that projects the displacement field onto a specific ansatz space and appropriately splits them into its polynomial and non-polynomial components.

2.2. Linear ansatz space and projection operator

As mentioned in the previous discussion, the approximated displacement functions in the space $\mathcal{L}(E)$ must be linear deformations and higher-order modes to converge the numerical solution monotonically. Therefore, let us first construct a space of linear displacements $\mathcal{P}(E) \subseteq \mathcal{L}(E)$ as follows

$$\mathcal{P} = \left\{ \mathbf{a} + \mathbf{B}(\mathbf{x} - \bar{\mathbf{x}}) : \mathbf{a} \in \mathbb{R}^2, \mathbf{B} \in \mathbb{R}^{2x2} \right\}, \tag{11}$$

where $\bar{x}$ is the centroid of element E. This space can be represented as the direct sum of the spaces of rigid body modes $\mathcal{R}(E)$ and constant strain rates $\mathcal{C}(E)$ defined by

$$\mathcal{R} = \left\{ \mathbf{a} + \mathbf{B}_{AS} \cdot (\mathbf{x} - \bar{\mathbf{x}}) : \mathbf{a} \in \mathbb{R}^2, \mathbf{B}_{AS} \in \mathbb{R}^{2x2}, \mathbf{B}_{AS}^T = -\mathbf{B}_{AS} \right\}, \tag{12}$$

$$\mathcal{R} = \left\{ \mathbf{B}_S \cdot (\mathbf{x} - \bar{\mathbf{x}}) : \mathbf{B}_S \in \mathbb{R}^{2x2}, \mathbf{B}_S^T = \mathbf{B}_S \right\}, \tag{13}$$

in which $\mathbf{B}$ is a second-order tensor which can be subdivided into symmetric tensor $\mathbf{B}_S$ and skew-symmetric tensor $\mathbf{B}_{AS}$.

The three following projection operators are defined to extract the components of the displacement field $\Pi_{\mathcal{R}} : \mathcal{L}(E) \to \mathcal{R}(E)$ for rigid body modes, $\Pi_{\mathcal{C}} : \mathcal{L}(E) \to \mathcal{C}(E)$ for constant strain states, and $\Pi_{\mathcal{P}} = \Pi_{\mathcal{R}} + \Pi_{\mathcal{C}}$ for the linear polynomial part. Thus, any functions $\mathbf{u}, \mathbf{v} \in \mathcal{L}(E)$ can be decomposed as

$$\mathbf{u} = \Pi_{\mathcal{P}}\mathbf{u} + (\mathbf{u} - \Pi_{\mathcal{P}}\mathbf{u}) = \Pi_{\mathcal{R}}\mathbf{u} + \Pi_{\mathcal{C}}\mathbf{u} + (\mathbf{u} - \Pi_{\mathcal{P}}\mathbf{u}), \tag{14}$$

$$\mathbf{v} = \Pi_{\mathcal{P}}\mathbf{v} + (\mathbf{v} - \Pi_{\mathcal{P}}\mathbf{v}) = \Pi_{\mathcal{R}}\mathbf{v} + \Pi_{\mathcal{C}}\mathbf{v} + (\mathbf{v} - \Pi_{\mathcal{P}}\mathbf{v}). \tag{15}$$

Here, $\Pi_{\mathcal{R}}\mathbf{u}, \Pi_{\mathcal{R}}\mathbf{v}$ are rigid body displacement, $\Pi_{\mathcal{C}}\mathbf{u}, \Pi_{\mathcal{C}}\mathbf{v}$ refer to constant strain states and $\mathbf{u} - \Pi_{\mathcal{P}}\mathbf{u}$, $\mathbf{v} - \Pi_{\mathcal{P}}\mathbf{v}$ stand for the higher-order components.

These projectors can be explicitly written as follows

$$\Pi_{\mathcal{R}}\mathbf{v} = \bar{v}_1\mathbf{r}_1 + \bar{v}_2\mathbf{r}_2 + \hat{\omega}_{12}\mathbf{r}_3, \tag{16}$$

$$\Pi_{\mathcal{C}}\mathbf{v} = \hat{\varepsilon}_{11}\mathbf{c}_1 + \hat{\varepsilon}_{22}\mathbf{c}_2 + \hat{\varepsilon}_{12}\mathbf{c}_3, \tag{17}$$

where $\bar{\mathbf{v}} = \dfrac{1}{n}\sum_{i=1}^{n}\mathbf{v}(\mathbf{x}_i)$ is the mean of values over the vertices of element E. The cell-average of the skew-symmetric gradient tensor is defined as $\hat{\boldsymbol{\omega}}(\mathbf{v}) = \dfrac{1}{2|E|}\displaystyle\int_{\partial E}(\mathbf{v} \otimes \mathbf{n} - \mathbf{n} \otimes \mathbf{v})\,\mathrm{d}s$, and the cell-average of the strain tensor is $\hat{\boldsymbol{\varepsilon}}(\mathbf{v}) = \dfrac{1}{2|E|}\displaystyle\int_{\partial E}(\mathbf{v} \otimes \mathbf{n} + \mathbf{n} \otimes \mathbf{v})\,\mathrm{d}s$. The basis vectors for space of rigid body modes are

$$\mathbf{r}_1 = \begin{bmatrix} 1 \\ 0 \end{bmatrix}, \mathbf{r}_2 = \begin{bmatrix} 0 \\ 1 \end{bmatrix}, \mathbf{r}_3 = \begin{bmatrix} x_2 - \bar{x}_2 \\ -(\quad x_1 - \bar{x}_1) \end{bmatrix}. \tag{18}$$

The basis vectors for space of constant strain state are

$$\mathbf{c}_1 = \begin{bmatrix} x_1 - \bar{x}_1 \\ 0 \end{bmatrix}, \quad \mathbf{c}_2 = \begin{bmatrix} 0 \\ x_2 - \bar{x}_2 \end{bmatrix}, \quad \mathbf{c}_3 = \begin{bmatrix} x_2 - \bar{x}_2 \\ x_1 - \bar{x}_1 \end{bmatrix}, \tag{19}$$

and the basis vectors for the space of polynomials are

$$\mathbf{p}_1 = \begin{bmatrix} 1 \\ 0 \end{bmatrix}, \mathbf{p}_2 = \begin{bmatrix} 0 \\ 1 \end{bmatrix}, \mathbf{p}_3 = \begin{bmatrix} x_1 - \bar{x}_1 \\ 0 \end{bmatrix}, \mathbf{p}_4 = \begin{bmatrix} x_2 - \bar{x}_2 \\ 0 \end{bmatrix}, \mathbf{p}_5 = \begin{bmatrix} 0 \\ x_1 - \bar{x}_1 \end{bmatrix}, \mathbf{p}_6 = \begin{bmatrix} 0 \\ x_2 - \bar{x}_2 \end{bmatrix}, \tag{20}$$

It is worth mentioning an essential property of the projector $\Pi_{\mathcal{P}}$ which satisfies the VEM approach is that for any $\mathbf{v} \in \mathcal{L}$, the higher-order component $\mathbf{v} - \Pi_{\mathcal{P}} v$ is energetically orthogonal to $\mathcal{P}$, which means

$$a_E(\mathbf{p}, \mathbf{v} - \Pi_{\mathcal{P}}\mathbf{v}) = 0, \quad \forall \mathbf{p} \in \mathcal{P}, \quad \forall \mathbf{v} \in \mathcal{L}. \tag{21}$$

2.3. Element stiffness matrix and force vectors

Following previous discussions on the kinematical decomposition of the displacements in Eqs. (14)–(15) and the energetically orthogonal condition in Eq. (21). The elemental bilinear operator can now be subdivided as follows

$$a_E(\mathbf{u}^h, \mathbf{v}^h) = a_E(\Pi_{\mathcal{C}}\mathbf{u}^h, \Pi_{\mathcal{C}}\mathbf{v}^h) + a_E(\mathbf{u}^h - \Pi_{\mathcal{P}}\mathbf{u}^h, \mathbf{v}^h - \Pi_{\mathcal{P}}\mathbf{v}^h). \tag{22}$$

The components of rigid body mode $\Pi_{\mathcal{R}}\mathbf{u}$ and $\Pi_{\mathcal{R}}\mathbf{v}$ do not contribute to this energy form due to its zero-strain deformation. The first term on the right-hand side of Eq. (22) was named the *consistency* component associated with the constant strain deformation, while the second term was called the *stability* component related to the non-polynomial functions. According to [50], this stability component is challenging to compute, which, in fact, can be replaced by an easy-computed crude approximation s_E without affecting the consistency energy

$$s_E(\mathbf{u}^h - \Pi_{\mathcal{P}}\mathbf{u}^h, \mathbf{v}^h - \Pi_{\mathcal{P}}\mathbf{v}^h) = \sum_i^n \alpha^e (\mathbf{u}^h - \Pi_{\mathcal{P}}\mathbf{u}^h) \cdot (\mathbf{v}^h - \Pi_{\mathcal{P}}\mathbf{v}^h), \tag{23}$$

where s_E must be positive definite bilinear form, and the scaling factor $\alpha^e > 0$ confirms the correct scaling of the higher-order mode energies. We finally obtained the bilinear form to proceed with the VEM element stiffness matrix

$$a_E(\mathbf{u}^h, \mathbf{v}^h) = a_E(\Pi_{\mathcal{C}}\mathbf{u}^h, \Pi_{\mathcal{C}}\mathbf{v}^h) + \sum_i^n \alpha^e (\mathbf{u}^h - \Pi_{\mathcal{P}}\mathbf{u}^h) \cdot (\mathbf{v}^h - \Pi_{\mathcal{P}}\mathbf{v}^h). \tag{24}$$

Let us go further into implementation detail by considering the polygonal element of N edges with nodal coordinates $\mathbf{x}_j$, nodal displacements $\mathbf{u}_j$,$\mathbf{v}_j$ and basis functions φ_j. The discrete form of Eqs. (16)–(17) can be written as

$$\Pi_{\mathcal{R}}\mathbf{v}^h = \mathbf{N}(\mathbf{H}_{\mathcal{R}}\mathbf{W}_{\mathcal{R}}^T)\mathbf{q}, \tag{25}$$

$$\Pi_{\mathcal{C}}\mathbf{v}^h = \mathbf{N}(\mathbf{H}_{\mathcal{C}}\mathbf{W}_{\mathcal{C}}^T)\mathbf{q}, \tag{26}$$

with

$$\mathbf{N} = \begin{bmatrix} \varphi_1 & 0 & \dots & \varphi_N & 0 \\ 0 & \varphi_1 & \dots & 0 & \varphi_N \end{bmatrix}, \tag{27}$$

$$\mathbf{q} = \begin{bmatrix} \mathbf{q}_{11} & \mathbf{q}_{21} & \cdots & \mathbf{q}_{1N} & \mathbf{q}_{2N} \end{bmatrix}^T, \tag{28}$$

$$\mathbf{H}_{\mathcal{R}} = \begin{bmatrix} 1 & 0 & x_{21} - \bar{x}_2 & \dots & 1 & 0 & x_{2N} - \bar{x}_2 \\ 0 & 1 & -(x_{11} - \bar{x}_1) & \dots & 0 & 1 & -(x_{1N} - \bar{x}_1) \end{bmatrix}^T, \tag{29}$$

$$\mathbf{H}_{\mathcal{C}} = \begin{bmatrix} x_{11} - \bar{x}_1 & 0 & x_{21} - \bar{x}_2 & \dots & x_{1N} - \bar{x}_1 & 0 & x_{2N} - \bar{x}_2 \\ 0 & x_{21} - \bar{x}_2 & x_{11} - \bar{x}_1 & \dots & 0 & x_{2N} - \bar{x}_2 & x_{1N} - \bar{x}_1 \end{bmatrix}^T, \tag{30}$$

$$\mathbf{W}_{\mathcal{R}} = \begin{bmatrix} \frac{1}{N} & 0 & q_{21} & \dots & \frac{1}{N} & 0 & q_{2N} \\ 0 & \frac{1}{N} & -q_{11} & \dots & 0 & \frac{1}{N} & -q_{1N} \end{bmatrix}^T, \tag{31}$$

$$\mathbf{W}_{\mathcal{C}} = \begin{bmatrix} 2q_{11} & 0 & q_{21} & \dots & 2q_{1N} & 0 & q_{2N} \\ 0 & 2q_{21} & q_{11} & \dots & 0 & 2q_{2N} & q_{1N} \end{bmatrix}^T, \tag{32}$$

and

$$\mathbf{q}_{i\alpha} = \frac{1}{2|E|} \int_{\partial E} \varphi_\alpha n_i = \frac{1}{4|E|} \left[|e_{\alpha-1}| (n_i)_{\alpha-1} + |e_\alpha| (n_i)_\alpha \right], \quad i = 1, 2. \tag{33}$$

Substitute Eqs. (25)–(32) into Eq. (24), we yield the matrix form

$$\begin{aligned} a_E \left(\mathbf{u}^h, \mathbf{v}^h \right) &= \mathbf{q}^T \left[|E| \mathbf{W}_{\mathcal{C}} \mathbf{C} \mathbf{W}_{\mathcal{C}}^T + \left(\mathbf{I} - \mathbf{P}_{\mathcal{P}} \right)^T \mathbf{S}_E \left(\mathbf{I} - \mathbf{P}_{\mathcal{P}} \right) \right] \mathbf{d} \\ &= \mathbf{q}^T \mathbf{k}_e \mathbf{d}, \end{aligned} \tag{34}$$

where $\mathbf{P}_{\mathcal{P}} = \mathbf{H}_{\mathcal{R}} \mathbf{W}_{\mathcal{R}}^T + \mathbf{H}_{\mathcal{C}} \mathbf{W}_{\mathcal{C}}^T$. The second (stability) term is roughly approximated by the internal energy entering with the discrepancy between a VEM shape function and its projection. The term $\left(\mathbf{I} - \mathbf{P}_{\mathcal{P}} \right)^T \left(\mathbf{I} - \mathbf{P}_{\mathcal{P}} \right)$ allows for this discrepancy, while $\mathbf{S}_E = \frac{|E| tr\left(\mathbf{C}\right)}{tr\left(\mathbf{H}_{\mathcal{C}}^T \mathbf{H}_{\mathcal{C}}\right)} \mathbf{I}$ scales the term concerning the consistency part, which directly affects the convergence of the method.

Similarly, the body force and the traction force vectors can be approximated by a piecewise constant. We then obtain

$$\begin{aligned} \mathbf{b}_E &= |E| \bar{\mathbf{N}}^T \hat{\mathbf{b}}, \\ \mathbf{t}_e &= |e| \bar{\mathbf{N}}_e^T \hat{\mathbf{t}}, \end{aligned} \tag{35}$$

in which

$$\bar{\mathbf{N}} = \begin{bmatrix} \frac{1}{N} & 0 & \dots \\ 0 & \frac{1}{N} & \dots \end{bmatrix}_{2\times 2N}, \quad \bar{\mathbf{N}}_e = \begin{bmatrix} \frac{1}{2} & 0 & \frac{1}{2} & 0 \\ 0 & \frac{1}{2} & 0 & \frac{1}{2} \end{bmatrix},$$

$$\hat{\mathbf{b}} = \frac{1}{|E|}\int_E \mathbf{b}\mathrm{d}\mathbf{x}, \quad \hat{\mathbf{t}} = \frac{1}{|e|}\int_e \mathbf{t}\mathrm{d}s.$$

The global stiffness matrix and global load vector are later assembled as in the standard FEM process whenever local matrices and local load vectors are computed for all elements in the discretized domain using Eqs. (34) and (35), respectively.

3. MULTI-MATERIAL PROPORTIONAL TOPOLOGY OPTIMIZATION WITH ORDERED SIMP ALGORITHM

3.1. Ordered SIMP algorithm

Zuo and Saitou [27] argued that the mass density values of solid material phases could be normalized by dividing the value of the heaviest material. By sorting them in ascending order, one has

$$0 \le \rho_1 \le \rho_2 \le \cdots \le \rho_I \le \cdots \le \rho_N = 1, \quad I = \overline{1, N}. \tag{36}$$

The normalized density field ρ within the interval $[0, 1]$ is then used as the design variable for topology optimization. The elastic modulus of each material phase is also normalized

$$\bar{E}_i = \frac{E_i}{E_N}. \tag{37}$$

It is noted that E_N is the elastic modulus of material N (the material with the highest value of normalized mass density), and it is not necessarily the largest elastic modulus. Normalization of material cost per unit weight is conducted in the same manner. When N materials are involved, the interval $[0, 1]$ of normalized density is divided into N segments. Within each segment, the elastic modulus is interpolated, e.g., using SIMP [3], hence the technique is named by Ordered SIMP. Compared to other techniques for multi-material topology optimization, such as extended SIMP [14, 15] or AAPA [19], Ordered SIMP does not introduce extra variables like extended SIMP and does not introduce extra sub-problems like AAPA. Therefore, the computational cost of Ordered SIMP remains low.

However, the interpolation scheme proposed by Zuo and Saitou [27] does not successfully resemble SIMP. Therefore, da Silveira and Palma [30] introduced a modified interpolation scheme for Ordered SIMP. Corresponding to a normalized density within

the sub-interval $[\rho_I, \rho_{I+1}]$, if material $I+1$ is stiffer than the material I, normalized elastic modulus is evaluated by

$$\bar{E}_e(\rho_e) = a(b(\rho_e - c))^p + d, \tag{38}$$

where p is the penalization factor. Coefficients a and b are the vertical and horizontal scaling coefficients, respectively, while c and d are the vertical and horizontal shift coefficients.

$$a = \bar{E}_{I+1} - \bar{E}_I, b = \frac{1}{\rho_{I+1} - \rho_I}, c = \rho_I, d = \bar{E}_I. \tag{39}$$

In case material I is stiffer than material $I+1$, the interpolation is given by

$$\bar{E}_e(\rho_e) = a(b(c - \rho_e))^p + d, \tag{40}$$

where

$$a = \bar{E}_I - \bar{E}_{I+1}, b = \frac{1}{\rho_{I+1} - \rho_I}, c = \rho_{I+1}, d = \bar{E}_{I+1}. \tag{41}$$

Similarly, if material $I+1$ is more expensive than the material I, interpolation of normalized cost is calculated as

$$\bar{C}_e(\rho_e) = a(b(c - \rho_e))^p + d, \tag{42}$$

where

$$a = \bar{C}_I - \bar{C}_{I+1}, b = \frac{1}{\rho_{I+1} - \rho_I}, c = \rho_{I+1}, d = \bar{C}_{I+1}. \tag{43}$$

If material I is more expensive than material I+1, the normalized cost is given by

$$\bar{C}_e(\rho_e) = a(b(\rho_e - c))^p + d, \tag{44}$$

where

$$a = \bar{C}_{I+1} - \bar{C}_I, b = \frac{1}{\rho_{I+1} - \rho_I}, c = \rho_I, d = \bar{C}_I. \tag{45}$$

Fig. 1 depicts the sketches of normalized elastic modulus and normalized cost with respect to normalized density obtained by the Zuo & Saitou scheme [27] and da Silveira & Palma scheme [30], in which three solid phases and one voided phase are involved. The corresponding normalized properties of materials are given in Table 1. A small value is assigned for the elastic modulus of the void (instead of zero) to avoid singularity during computation.

Table 1. Material properties for four-phase design [30]

	Void	MAT1 (GREEN)	MAT2 (BLUE)	MAT3 (RED)
Normalized density	0	0.4	0.6	1.0
Normalized elastic modulus	10^{-9}	0.5	0.7	1.0
Normalized cost	0	1.6	1.2	1.0

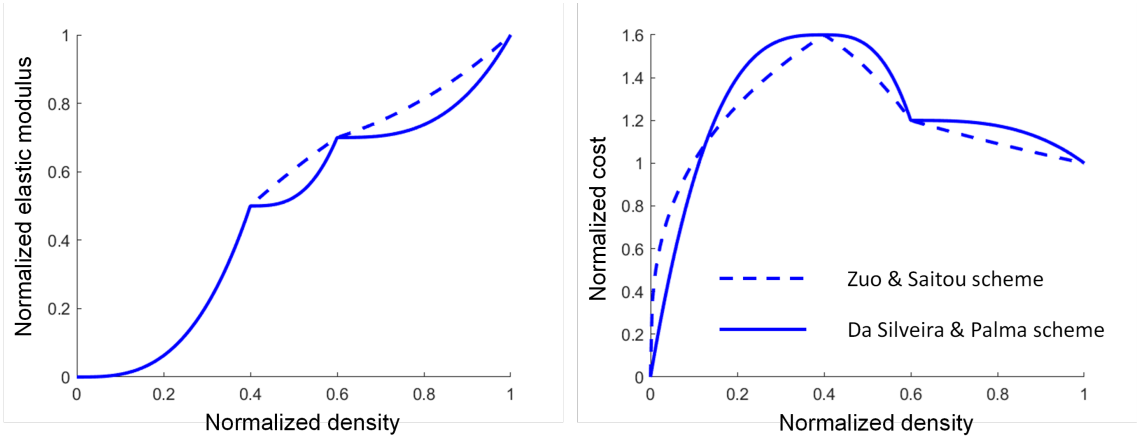

Fig. 1. Graphs of normalized elastic modulus and normalized cost (per unit weight) with respect to normalized density

3.2. Multi-material Proportional Topology Optimization using Ordered SIMP algorithm

The mathematical statement for the compliance minimization problem is given as follows:

Find:

$$\rho_e \in [0,1], (e = 1,2,3,\ldots,NE). \tag{46}$$

Objective:

$$\text{minimize } f = \mathbf{u}^T \mathbf{K}(\rho_e)\mathbf{u}. \tag{47}$$

Subject to:

Equilibrium:

$$\mathbf{K}(\rho_e)\mathbf{u} = \mathbf{F}. \tag{48}$$

Mass constraint:

$$\sum_e \rho_e V_e \leq \bar{m}|\Omega|. \tag{49}$$

Cost constraint:

$$\sum_e \bar{C}_e \rho_e V_e \leq \bar{C}|\Omega|. \tag{50}$$

Here, design variables are element-based defined, i.e., each design variable ρ_e is associated with one element e, and NE is the number of elements. Eq. (48) is the equilibrium equation, where $\mathbf{K}$ is the global stiffness matrix, $\mathbf{u}$ is the displacement vector and $\mathbf{F}$ is global force vector. The constraints on normalized mass and normalized cost are given

in Eqs. (49) and (50), in which $\bar{m}$ and $\bar{C}$ are the predefined mass fraction and cost fraction, respectively. V_e is the elemental area while $|\Omega|$ is the total area (or total volume for three-dimensional cases) of the design domain.

The general algorithm of Proportional Topology Optimization (PTO) [41] is depicted as a flowchart in Fig. 2. In every global iteration, the Virtual Element Analysis is implemented first with the obtained material distribution, and then the compliance objective function in Eq. (47) is calculated as an input of our update scheme. The main target of the update scheme is to distribute the material via an inner loop, such that each material receives an amount of material proportionally to its contribution to the objective function. The target amount of material (the total amount of material to be distributed) is set as TM. The inner loop is given by [41] as follows

$$\rho_e = \frac{f_e}{\sum_{j=1}^{NE}(f_j V_j)} RM, \tag{51}$$

where RM is the remaining material, and the elemental compliance energy $f_e = \mathbf{u_e}^T \mathbf{K_e}(\rho_e)\mathbf{u_e}$. At the beginning of the inner loop, $RM = TM$, and is updated by

$$RM = TM - \sum_{e=1}^{NE} \rho_e V_e. \tag{52}$$

The inner loop stops when RM is less than a tolerance, for e.g., $RM \leq 10^{-4} TM$.

In order to avoid the "checkerboard" issue, a density filter is applied [41,56]

$$\hat{\rho}_e = \frac{\sum w_{ej}\rho_j}{\sum w_{ej}}, \quad 0 \leq \rho_e \leq 1, \tag{53}$$

where $\hat{\rho}_e$ is the filtered density associated with element e, while ρ_j is the non-filtered density associated with element j. In fact, the weights could be determined by any decreasing function with respect to the distance from the center of element e. Here, the weights w_{ej} is simply given by

$$w_{ej} = \begin{cases} \dfrac{r_0 - r_{ej}}{r_0}, & \text{for } r_{ej} < r_0 \\ 0, & \text{otherwise} \end{cases} \tag{54}$$

where r_0 is a user-defined filter radius, and r_{ej} is the distance between the centers of element e and element j. Taking the fact that an unstructured mesh is utilized, r_0 is not set as a constant in this paper, but it is dependent on the element size. Particularly, for an arbitrary element e, we chose $r_0 = 3\ R_e$, where R_e is defined as the average distance from the element center to its vertexes.

If only mass constraint is of concern, the target amount of material TM could be kept as the required mass fraction, $TM = \bar{m}|\Omega|$. However, when both mass and cost constraints are enforced, adjustment on TM is needed. In every (global) iteration, if the

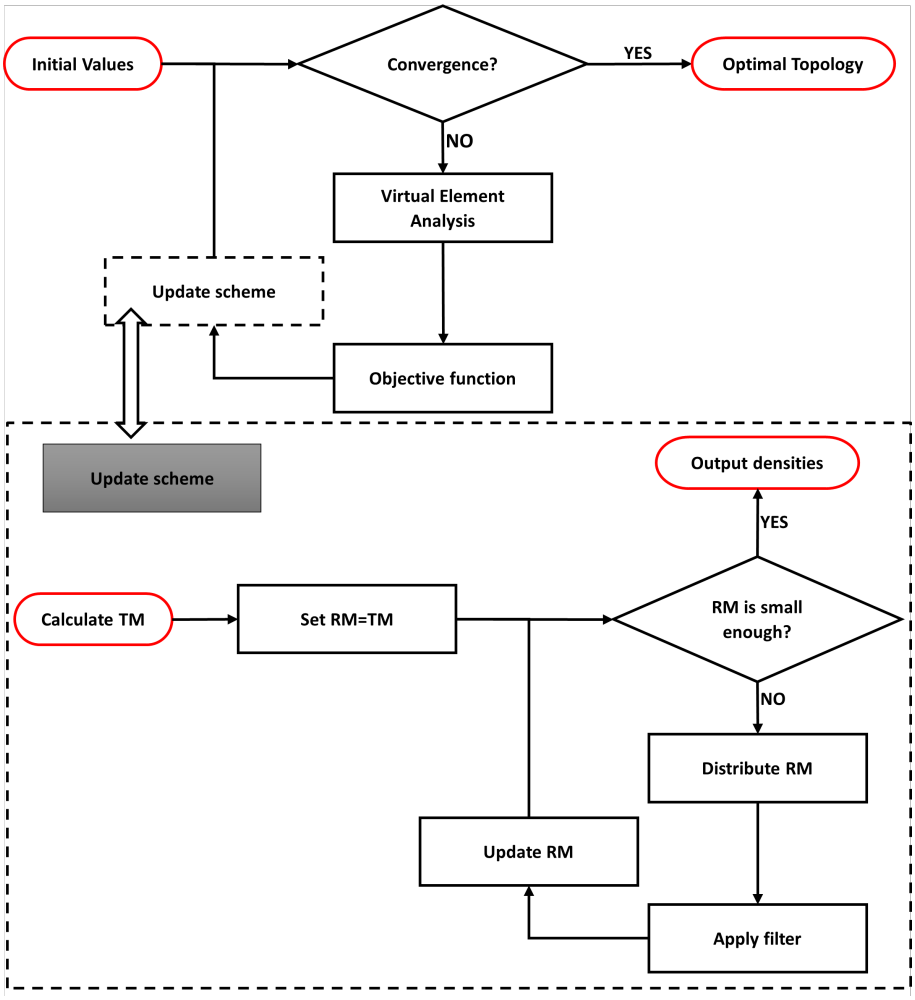

Fig. 2. The general Proportional Topology Optimization including update scheme

total normalized cost is higher than the allowed value, TM is reduced; otherwise TM is increased, but TM should not violate the mass constraint. In short, the target amount of material is adjusted such that the mass fraction or cost fraction will be equal to the required limit value while the other constraint is also satisfied. The preference for lower cost is further reflected in the material distribution by modification of Eq. (51) as

$$\rho_e = \frac{\frac{f_e}{\bar{C}_e}}{\sum_{j=1}^{NE} \frac{f_j}{\bar{C}_j} V_j} RM. \tag{55}$$

Eq. (51) is interpreted that material will be distributed into an element e proportionally to its compliance value evaluated and inverse proportionally to its cost value.

After the PTO inner loop, the normalized densities (design variables) are finally calculated by

$$\rho_{t+1} = \alpha\rho_t + (1-\alpha)\rho_{new}, \tag{56}$$

in which ρ_t is the vector of normalized densities of the previous iteration and the newly calculated values by PTO, ρ_{new}. Coefficient α controls the weight of ρ_t and ρ_{new}. Here, $\alpha = 0.5$ is taken.

4. NUMERICAL EXAMPLES

In this section, the four-phase design of two benchmark examples is considered, the Messerschmitt-Bölkow-Blohm (MBB) beam problem and the annular disc being tangentially loaded problem, using the artificial material properties given in Table 1. The results obtained by the PTO algorithm are compared with those obtained by the well-known Method of Moving Asymptotes algorithm (MMA) [58]. The implementation of the MMA-based approach is based on the computer code publicly provided by da Silveira & Palma [30], in which the finite element analysis using a uniform mesh of unit square elements is replaced by the virtual element analysis using unstructured polygonal mesh obtained by the tool PolyMesher [58]. It is worth mentioning that the topology optimization results obtained in these numerical examples can be taken into 3D printing for fabrication by a further post-processing step. This step will improve the discreteness of the density field by considering the Heaviside-type projection-based volume-preserving density filter [57].

For comparison purposes, the numerical aspects for both approaches (PTO and MMA) should be kept as close as possible, such as the same mesh, same density filter, and same stopping criterion. The stopping criterion is that either the maximum number of iterations (500) is reached or the relative change between objective values of 9 consecutive iterations is less than 10^{-4}. The blending between history values and values of design variables newly calculated by the optimizer (Eq. (56)) is used for both PTO and MMA.

In fact, the difference between the two approaches is the inner loop for updating the design variables, i.e., PTO and MMA algorithms. For the MMA algorithm, the derivative information of the objective function and the constraints (mass and cost constraints) with respect to each design variable must be computed. Such derivative information is not required by the PTO algorithm, as presented in Section 3.2. Furthermore, following the suggestion in [30], a continuation scheme for the penalization factor p (see Eq. (38)) is employed for MMA. The continuation scheme is conducted by increasing p from 1 to 3 with increment size $\Delta p = 0.5$. Each value of p will be run with at most 100 iterations. For the PTO-based approach, the continuation scheme of p is not needed; hence a constant value $p = 3$ is used.

4.1. Four-phase design of a Messerschmitt-Bölkow-Blohm (MBB) beam

Four-phase design of the Messerschmitt-Bölkow-Blohm (MBB) beam problem (see the sketch in Fig. 3) is investigated. Due to symmetry, only one-half of the beam is modelled in numerical analysis. Both mass fraction and cost fraction must not exceed 0.32. A mesh of 1800 unstructured polygonal virtual elements is used.

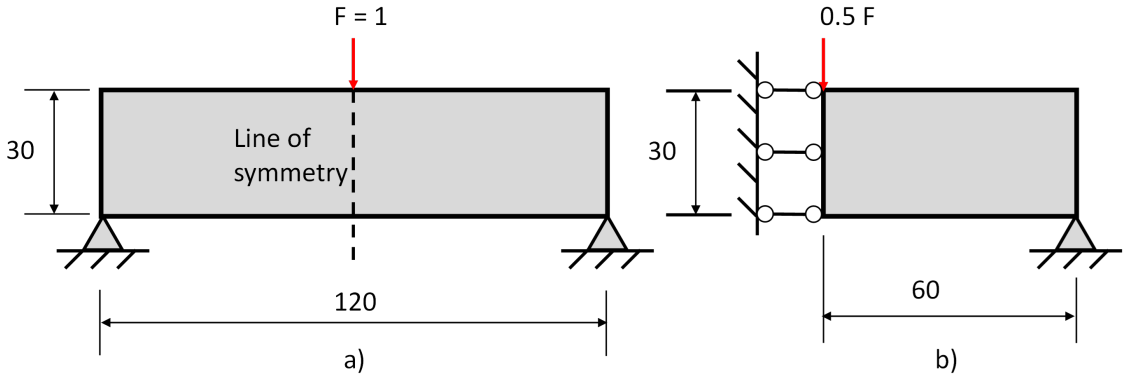

Fig. 3. Sketch of MBB beam: a) Full model, b) Half model due to symmetry

Results obtained by the PTO algorithm and the Method of Moving Asymptotes (MMA) are given in Table 2, while the two designs are depicted in Fig. 4. The historical curves for cost fraction and mass fraction are presented in Fig. 5. The procedures for both methods are nearly identical (same finite element mesh, same density filter, same stopping criterion). The only difference is the update scheme, PTO algorithm and MMA algorithm. Furthermore, we also made a comparison in Table 3 to see the effect of the PTO algorithm under different constraints. The key difference is that the mass constraint produces a stiffer structure but higher cost, while the mass and cost constraints give us more flexibility in multi-constrained problems. This is a trade-off. In the case of lightweight structural design without caring about the cost; we only need to consider mass constraint. On the other hand, when saving cost is also an important factor during design, enforcement of both mass and cost constraints would be a suitable option for designers.

Table 2. Results for the MBB beam

	Iterations	Compliance	Time	Mass fraction	Cost fraction
MMA	423	35.17	∼292 s	0.248	0.257
PTO	210	33.65	∼135 s	0.261	0.320

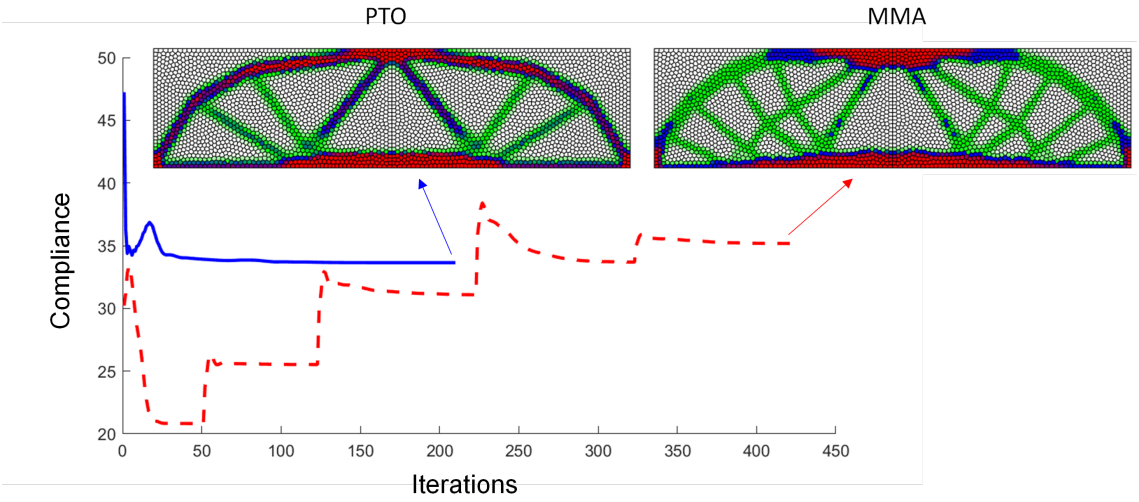

Fig. 4. Designs obtained for the MBB beam

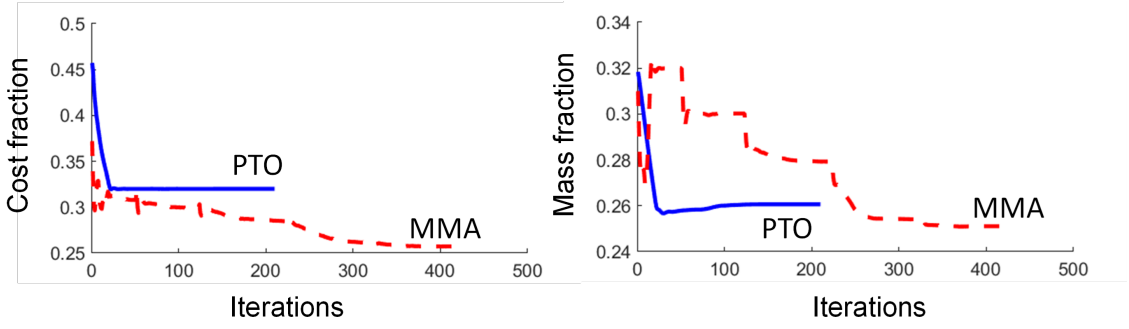

Fig. 5. Historical curves for cost fraction and mass fraction of the MBB beam

Table 3. Comparison among different constraints for the MBB beam

	Iterations	Compliance	Mass fraction	Cost fraction
Mass constraint	78	26.87	0.320	0.383
Mass and Cost constraints	210	33.65	0.261	0.320

It is observed that the design by MMA has lower values of cost fraction and mass fraction, but the design by PTO has lower values of compliance. This observation reflects the different behavior of the two optimizers (PTO and MMA). In PTO, we adjust the target amount of material such that either the mass fraction or cost fraction will be equal to the required value while the other is simultaneously satisfied. Such adjustment does not necessarily occur in MMA. This is possibly the reason that MMA could provide design

with both lighter weight and lower cost. However, the objective here is the minimization of structural compliance. Computational time by MMA is more significant, mainly because of the larger number of iterations. The average computational time for each iteration (dividing the total time by the number of iterations) is nearly equivalent for the two algorithms. Critically, it should be emphasized that comparison between approaches of topology optimization is not trivial. Reference [59] suggested that for conservative assessment, the results of topology optimization should be thresholded to 0-1 solution, for example, by Heaviside-type projection. In this paper, Heaviside-type projection is not taken into account, but a discussion on the employment of the projection in the PTO scheme for single material problems can be found in [43, 57].

A common tendency is observed in the designs of the two approaches (PTO and MMA) in Fig. 4. Both optimizers tend to select the stiff material phase (the Red phase) in regions with loads or constraints on displacements. This is reasonable and consistent with observations reported by previous works [22, 60], which used a different technique for multi-material problems, namely AAPA.

4.2. Four-phase design of an annular disc being tangentially loaded

In this example, the problem of an annular disc being tangentially loaded is studied. A sketch of the geometry and boundary conditions of the problem is presented in Fig. 6. Due to anti-symmetry, a quarter of the disc is modelled for numerical analysis. The artificial material properties in Table 1 are taken. For this problem, the design domain is discretized into 1800 unstructured polygonal virtual elements. The mass fraction and cost fraction are required not to exceed 0.5.

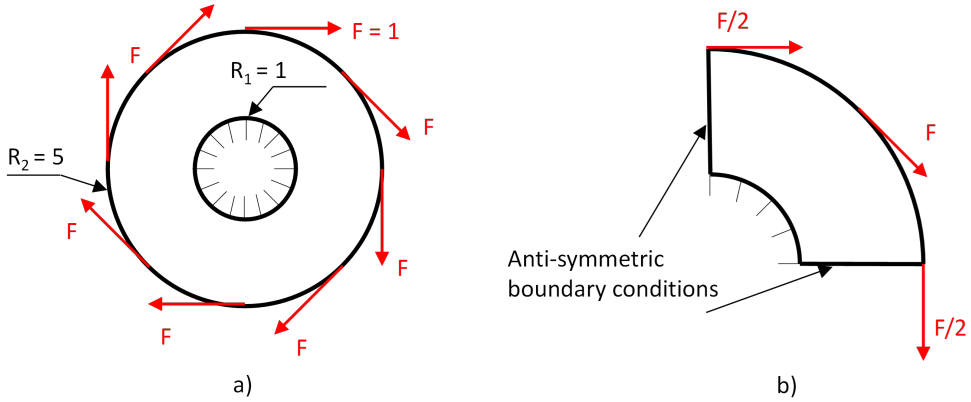

Fig. 6. Sketch of annular disc being tangentially loaded:
a) Full model, b) Quarter model due to anti-symmetry

The results from two approaches, PTO and MMA, are reported in Table 4 and Fig. 7. Again, more iterations are needed by MMA. The historical curves of mass fraction and cost fraction are further depicted in Fig. 8. For this particular problem, the compliance value, the mass fraction and the cost fraction given by MMA are all lower than the corresponding values by PTO. However, the differences are small.

Table 4. Results for the annular disc

	Iterations	Compliance	Time	Mass fraction	Cost fraction
MMA	382	112.39	∼246 s	0.423	0.47
PTO	108	114.48	∼66 s	0.428	0.5

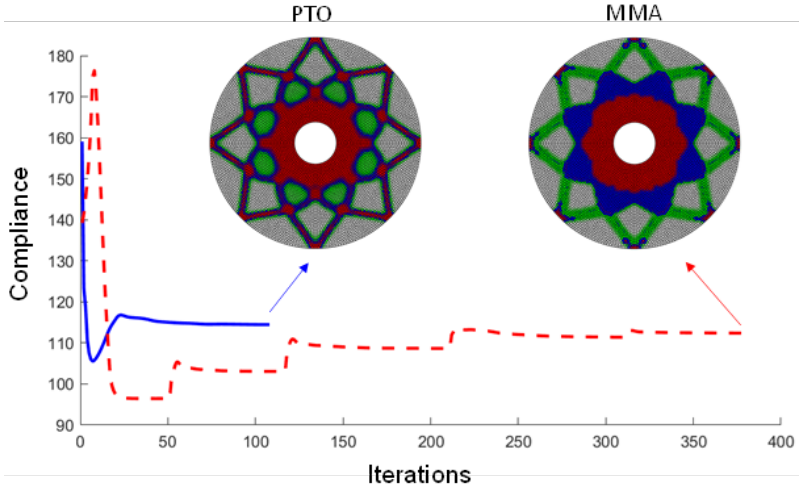

Fig. 7. Designs obtained for the annular disc being tangentially loaded

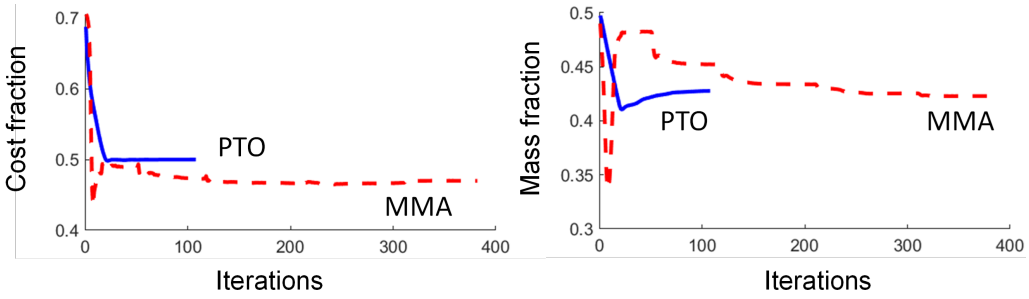

Fig. 8. Historical curves for cost fraction and mass fraction of the annular disc being tangentially loaded

As can be seen in Fig. 7, the Red phase, which has the highest elastic modulus, is chosen by both optimizers in regions where stress concentration occurs, i.e. the location of loads and displacement restriction.

5. CONCLUSION

The Ordered SIMP technique has been successfully integrated into the Proportional Topology Optimization (PTO) algorithm, resulting in a novel approach for problems that involve multiple materials. A characteristic of the PTO is that the derivative of the shape function with respect to design variables is not needed. Instead, the material is distributed proportionally to the contribution of each element in the total structural compliance (objective function). This update scheme is indeed heuristic, but it is this heuristic property that makes the algorithm simple to understand and implement.

The advantage of Ordered SIMP would be the fact that multi-material topology optimization can be conducted without introducing additional variables. Hence, compared to previous works on the application of PTO for multi-material problems, the current approach has the advantage of low computational effort.

Furthermore, it is worth noting that in the available kinds of literature, the PTO algorithm is only used for problems involving one type of constraint, e.g., volume or stress. In this paper, a new material distribution scheme (Eq. (55)) is proposed such that two types of constraint, i.e., mass and cost constraints, can be simultaneously considered by PTO. The results obtained by PTO are comparable with those by the well-known Method of Asymptotes (MMA). Nevertheless, it is realized that the behaviors of the two algorithms (PTO and MMA) are different. For the proposed PTO scheme, the amount of material is adjusted such that either the mass fraction or cost fraction is equal to the required (upper bound) value. Such adjustment does not necessarily occur in MMA, resulting in designs that possibly have both lower mass and cost fractions, although the compliance values from the designs by MMA and PTO are not much different. Less computational time is needed by PTO, at least in the examples being considered.

For structural analysis, the Virtual Element Method (VEM) with unstructured polygonal mesh is used, instead of the usual Finite Element Method (FEM). Compared to triangular or quadrilateral meshes, an unstructured polygonal mesh (in the context of topology optimization) has the advantage that the single node-connections can be automatically avoided. Compared to FEM for polygonal meshes, VEM could be more efficiently implemented since no numerical integration is required, at least when the assumption of small deformation and linear elasticity holds.

DECLARATION OF COMPETING INTEREST

The authors declare that they have no known competing financial interests or personal relationships that could have appeared to influence the work reported in this paper.

ACKNOWLEDGMENT

This research is funded by the Vietnamese-German University under grant number DTCS2022-001.

REFERENCES

[1] M. P. Bendsoe and N. Kikuchi. Generating optimal topologies in structural design using a homogenization method. *Computer Methods in Applied Mechanics and Engineering*, **71**, (1988), pp. 197–224. https://doi.org/10.1016/0045-7825(88)90086-2.

[2] M. P. Bendsoe. Optimal shape design as a material distribution problem. *Structural Optimization*, **1**, (4), (1989), pp. 193–202. https://doi.org/10.1007/BF01650949.

[3] O. Sigmund. A 99-line topology optimization code written in Matlab. *Structural and Multidisciplinary Optimization*, **21**, (2), (2001), pp. 120–127. https://doi.org/10.1007/s001580050176.

[4] M. Stolpe and K. Svanberg. An alternative interpolation scheme for minimum compliance topology optimization. *Structural and Multidisciplinary Optimization*, **22**, (2), (2001), pp. 116–124. https://doi.org/10.1007/s001580100129.

[5] M. Y. Wang, X. Wang, and D. Guo. A level set method for structural topology optimization. *Computer Methods in Applied Mechanics and Engineering*, **192**, (1-2), (2003), pp. 227–246. https://doi.org/10.1016/s0045-7825(02)00559-5.

[6] V. J. Challis. A discrete level-set topology optimization code written in Matlab. *Structural and Multidisciplinary Optimization*, **41**, (3), (2009), pp. 453–464. https://doi.org/10.1007/s00158-009-0430-0.

[7] P. Wei, Z. Li, X. Li, and M. Y. Wang. An 88-line MATLAB code for the parameterized level set method based topology optimization using radial basis functions. *Structural and Multidisciplinary Optimization*, **58**, (2), (2018), pp. 831–849. https://doi.org/10.1007/s00158-018-1904-8.

[8] A. Takezawa, S. Nishiwaki, and M. Kitamura. Shape and topology optimization based on the phase field method and sensitivity analysis. *Journal of Computational Physics*, **229**, (7), (2010), pp. 2697–2718. https://doi.org/10.1016/j.jcp.2009.12.017.

[9] L. Dede, M. J. Borden, and T. J. R. Hughes. Isogeometric analysis for topology optimization with a phase field model. *Archives of Computational Methods in Engineering*, **19**, (3), (2012), pp. 427–465. https://doi.org/10.1007/s11831-012-9075-z.

[10] W. Zhang, J. Yuan, J. Zhang, and X. Guo. A new topology optimization approach based on Moving Morphable Components (MMC) and the ersatz material model. *Structural and Multidisciplinary Optimization*, **53**, (6), (2015), pp. 1243–1260. https://doi.org/10.1007/s00158-015-1372-3.

[11] W. Zhang, D. Li, J. Zhou, Z. Du, B. Li, and X. Guo. A Moving Morphable Void (MMV)-based explicit approach for topology optimization considering stress constraints. *Computer Methods in Applied Mechanics and Engineering*, **334**, (2018), pp. 381–413. https://doi.org/10.1016/j.cma.2018.01.050.

[12] J. A. Norato, B. K. Bell, and D. A. Tortorelli. A geometry projection method for continuum-based topology optimization with discrete elements. *Computer Methods in Applied Mechanics and Engineering*, **293**, (2015), pp. 306–327. https://doi.org/10.1016/j.cma.2015.05.005.

[13] H. Smith and J. Norato. A MATLAB code for topology optimization using the geometry projection method. *Structural and Multidisciplinary Optimization*, **62**, (3), (2020), pp. 1579–1594. https://doi.org/10.1007/s00158-020-02552-0.

[14] C. F. Hvejsel and E. Lund. Material interpolation schemes for unified topology and multi-material optimization. *Structural and Multidisciplinary Optimization*, **43**, (6), (2011), pp. 811–825. https://doi.org/10.1007/s00158-011-0625-z.

[15] D. Li and I. Y. Kim. Multi-material topology optimization for practical lightweight design. *Structural and Multidisciplinary Optimization*, **58**, (3), (2018), pp. 1081–1094. https://doi.org/10.1007/s00158-018-1953-z.

[16] M. Y. Wang and X. Wang. "Color" level sets: a multi-phase method for structural topology optimization with multiple materials. *Computer Methods in Applied Mechanics and Engineering*, **193**, (6-8), (2004), pp. 469–496. https://doi.org/10.1016/j.cma.2003.10.008.

[17] Y. Wang, Z. Luo, Z. Kang, and N. Zhang. A multi-material level set-based topology and shape optimization method. *Computer Methods in Applied Mechanics and Engineering*, **283**, (2015), pp. 1570–1586. https://doi.org/10.1016/j.cma.2014.11.002.

[18] S. Zhou and M. Y. Wang. Multimaterial structural topology optimization with a generalized Cahn-Hilliard model of multiphase transition. *Structural and Multidisciplinary Optimization*, **33**, (2), (2006), pp. 89–111. https://doi.org/10.1007/s00158-006-0035-9.

[19] R. Tavakoli and S. M. Mohseni. Alternating active-phase algorithm for multimaterial topology optimization problems: a 115-line MATLAB implementation. *Structural and Multidisciplinary Optimization*, **49**, (4), (2014), pp. 621–642. https://doi.org/10.1007/s00158-013-0999-1.

[20] K. N. Chau, K. N. Chau, T. Ngo, K. Hackl, and H. Nguyen-Xuan. A polytree-based adaptive polygonal finite element method for multi-material topology optimization. *Computer Methods in Applied Mechanics and Engineering*, **332**, (2018), pp. 712–739. https://doi.org/10.1016/j.cma.2017.07.035.

[21] J. Park, T. H. Nguyen, J. J. Shah, and A. Sutradhar. Conceptual design of efficient heat conductors using multi-material topology optimization. *Engineering Optimization*, **51**, (5), (2018), pp. 796–814. https://doi.org/10.1080/0305215x.2018.1497613.

[22] M. N. Nguyen and T. Q. Bui. Multi-material gradient-free proportional topology optimization analysis for plates with variable thickness. *Structural and Multidisciplinary Optimization*, **65**, (2022). https://doi.org/10.1007/s00158-022-03176-2.

[23] W. Sha, M. Xiao, L. Gao, and Y. Zhang. A new level set based multi-material topology optimization method using alternating active-phase algorithm. *Computer Methods in Applied Mechanics and Engineering*, **377**, (2021). https://doi.org/10.1016/j.cma.2021.113674.

[24] A. Habibian and Sohouli. Multi-material topology optimization of structures with discontinuities using Peridynamics. *Composite Structures*, **258**, (2021). https://doi.org/10.1016/j.compstruct.2020.113345.

[25] Z. Han, K. Wei, Z. Gu, X. Ma, and X. Yang. Stress-constrained multi-material topology optimization via an improved alternating active-phase algorithm. *Engineering Optimization*, **54**, (2), (2021), pp. 305–328. https://doi.org/10.1080/0305215x.2020.1867119.

[26] M. N. Nguyen, M. T. Tran, H. Q. Nguyen, and T. Q. Bui. A multi-material proportional topology optimization approach for compliant mechanism problems. *European Journal of Mechanics - A/Solids*, **100**, (2023). https://doi.org/10.1016/j.euromechsol.2023.104957.

[27] W. Zuo and K. Saitou. Multi-material topology optimization using ordered SIMP interpolation. *Structural and Multidisciplinary Optimization*, **55**, (2), (2016), pp. 477–491. https://doi.org/10.1007/s00158-016-1513-3.

[28] S. Xu, J. Liu, B. Zou, Q. Li, and Y. Ma. Stress constrained multi-material topology optimization with the ordered SIMP method. *Computer Methods in Applied Mechanics and Engineering*, **373**, (2021). https://doi.org/10.1016/j.cma.2020.113453.

[29] X. Gu, S. He, Y. Dong, and T. Song. An improved ordered SIMP approach for multi-scale concurrent topology optimization with multiple microstructures. *Composite Structures*, **287**, (2022). https://doi.org/10.1016/j.compstruct.2022.115363.

[30] O. A. A. Silveira and L. F. Palma. Some considerations on multi-material topology optimization using ordered SIMP. *Structural and Multidisciplinary Optimization*, **65**, (9), (2022). https://doi.org/10.1007/s00158-022-03379-7.

[31] C.-Y. Wu and K.-Y. Tseng. Topology optimization of structures using modified binary differential evolution. *Structural and Multidisciplinary Optimization*, **42**, (6), (2010), pp. 939–953. https://doi.org/10.1007/s00158-010-0523-9.

[32] J. F. A. Madeira, H. Rodrigues, and H. Pina. Multi-objective optimization of structures topology by genetic algorithms. *Advances in Engineering Software*, **36**, (1), (2005), pp. 21–28. https://doi.org/10.1016/j.advengsoft.2003.07.001.

[33] G.-C. Luh, C.-Y. Lin, and Y.-S. Lin. A binary particle swarm optimization for continuum structural topology optimization. *Applied Soft Computing*, **11**, (2), (2011), pp. 2833–2844. https://doi.org/10.1016/j.asoc.2010.11.013.

[34] O. Sigmund. On the usefulness of non-gradient approaches in topology optimization. *Structural and Multidisciplinary Optimization*, **43**, (5), (2011), pp. 589–596. https://doi.org/10.1007/s00158-011-0638-7.

[35] D. Guirguis and M. F. Aly. A derivative-free level-set method for topology optimization. *Finite Elements in Analysis and Design*, **120**, (2016), pp. 41–56. https://doi.org/10.1016/j.finel.2016.06.002.

[36] D. Guirguis, W. W. Melek, and M. F. Aly. High-resolution non-gradient topology optimization. *Journal of Computational Physics*, **372**, (2018), pp. 107–125. https://doi.org/10.1016/j.jcp.2018.06.025.

[37] P. Liu, Y. Yan, X. Zhang, Y. Luo, and Z. Kang. Topological design of microstructures using periodic material-field series-expansion and gradient-free optimization algorithm. *Materials & Design*, **199**, (2021). https://doi.org/10.1016/j.matdes.2020.109437.

[38] B. Bochenek and K. Tajs-Zielinska. GOTICA - generation of optimal topologies by irregular cellular automata. *Structural and Multidisciplinary Optimization*, **55**, (6), (2017). https://doi.org/10.1007/s00158-016-1614-z.

[39] D. C. Da, J. H. Chen, X. Y. Cui, and G. Y. Li. Design of materials using hybrid cellular automata. *Structural and Multidisciplinary Optimization*, **56**, (1), (2017), pp. 131–137. https://doi.org/10.1007/s00158-017-1652-1.

[40] J. Jia, D. Da, C.-L. Loh, H. Zhao, S. Yin, and J. Xu. Multi-scale topology optimization for non-uniform microstructures with hybrid cellular automata. *Structural and Multidisciplinary Optimization*, **62**, (2), (2020), pp. 757–770. https://doi.org/10.1007/s00158-020-02533-3.

[41] E. Biyikli and A. C. To. Proportional Topology Optimization: A new non-sensitivity method for solving stress constrained and minimum compliance problems and its implementation in MATLAB. *PLOS ONE*, **10**, (12), (2015). https://doi.org/10.1371/journal.pone.0145041.

[42] H. Wang, W. Cheng, R. Du, S. Wang, and Y. Wang. Improved proportional topology optimization algorithm for solving minimum compliance problem. *Structural and Multidisciplinary Optimization*, **62**, (2020), pp. 475–493. https://doi.org/10.1007/s00158-020-02504-8.

[43] W. Cheng, H. Wang, M. Zhang, and R. Du. Improved proportional topology optimization algorithm for minimum volume problem with stress constraints. *Engineering Computations*, **38**, (1), (2020), pp. 392–412. https://doi.org/10.1108/ec-12-2019-0560.

[44] Z. Ullah, B. Ullah, W. Khan, and S. Islam. Proportional topology optimization with maximum entropy-based meshless method for minimum compliance and stress constrained problems. *Engineering with Computers*, **38**, (6), (2022), pp. 5541–5561. https://doi.org/10.1007/s00366-022-01683-w.

[45] M. Cui, Y. Zhang, X. Yang, and C. Luo. Multi-material proportional topology optimization based on the modified interpolation scheme. *Engineering with Computers*, **34**, (2017), pp. 287–305. https://doi.org/10.1007/s00366-017-0540-z.

[46] C. Talischi, G. H. Paulino, A. Pereira, and I. F. M. Menezes. Polygonal finite elements for topology optimization: A unifying paradigm. *International Journal for Numerical Methods in Engineering*, **82**, (6), (2009), pp. 671–698. https://doi.org/10.1002/nme.2763.

[47] L. B. Veiga, F. Brezzi, A. Cangiani, G. Manizini, L. D. Marini, and A. Russo. Basis principles of virtual element methods. *Mathematical Models and Methods in Applied Sciences*, **23**, (1), (2012), pp. 199–214. https://doi.org/10.1142/s0218202512500492.

[48] L. B. Veiga, F. Brezzi, and L. D. Marini. Virtual elements for linear elasticity problems. *SIAM Journal on Numerical Analysis*, **51**, (2013), pp. 794–812. https://doi.org/10.1137/120874746.

[49] H. Chi, A. Pereira, I. F. M. Menezes, and G. H. Paulino. Virtual element method (VEM)-based topology optimization: an integrated framework. *Structural and Multidisciplinary Optimization*, **62**, (3), (2019), pp. 1089–1114. https://doi.org/10.1007/s00158-019-02268-w.

[50] A. L. Gain, C. Talischi, and G. H. Paulino. On the Virtual Element Method for three-dimensional linear elasticity problems on arbitrary polyhedral meshes. *Computer Methods in Applied Mechanics and Engineering*, **282**, (2014), pp. 132–160. https://doi.org/10.1016/j.cma.2014.05.005.

[51] A. Ortiz-Bernardin, C. Alvarez, N. Hitschfeld-Kahler, A. Russo, R. Silva-Valenzuela, and E. Olate-Sanzana. Veamy: an extensible object-oriented C++ library for the virtual element method. *Numerical Algorithms*, **82**, (2019), pp. 1189–1220. https://doi.org/10.1007/s11075-018-00651-0.

[52] H. Chi, L. B. Veiga, and G. H. Paulino. Some basic formulations of the virtual element method (VEM) for finite deformations. *Computer Methods in Applied Mechanics and Engineering*, **318**, (2017), pp. 148–192. https://doi.org/10.1016/j.cma.2016.12.020.

[53] E. Artioli, L. B. Veiga, C. Lovadina, and E. Sacco. Arbitrary order 2D virtual elements for polygonal meshes: Part II, inelastic problem. *Computational Mechanics*, **60**, (4), (2017), pp. 643–657. https://doi.org/10.1007/s00466-017-1429-9.

[54] P. Wriggers, W. T. Rust, and B. D. Reddy. A virtual element method for contact. *Computational Mechanics*, **58**, (6), (2016), pp. 1039–1050. https://doi.org/10.1007/s00466-016-1331-x.

[55] M. F. Benedetto, A. Caggiano, and G. Etse. Virtual elements and zero thickness interface-based approach for fracture analysis of heterogeneous materials. *Computer Methods in Applied Mechanics and Engineering*, **338**, (2018), pp. 41–67. https://doi.org/10.1016/j.cma.2018.04.001.

[56] P. F. Antonieti, M. Bruggi, S. Scacchi, and M. Verani. On the virtual element method for topology optimization on polygonal meshes: A numerical study. *Computers & Mathematics with Applications*, **74**, (5), (2017), pp. 1091–1109. https://doi.org/10.1016/j.camwa.2017.05.025.

[57] T. M. Tuan, M. N. Nguyen, T. Q. Bui, and H. Q. Nguyen. An enhanced proportional topology optimization with virtual elements: Formulation and numerical implementation. *Finite Elements in Analysis and Design*, **222**, (2023). https://doi.org/10.1016/j.finel.2023.103958.

[58] C. Talischi, G. H. Paulino, A. Pereira, and I. F. M. Menezes. PolyMesher: A general-purpose mesh generator for polygonal elements written in Matlab. *Structural and Multidisciplinary Optimization*, **45**, (3), (2012), pp. 309–328. https://doi.org/10.1007/s00158-011-0706-z.

[59] O. Sigmund. On benchmarking and good scientific practise in topology optimization. *Structural and Multidisciplinary Optimization*, **65**, (2022). https://doi.org/10.1007/s00158-022-03427-2.

[60] T. T. Banh and D. Lee. Topology optimization of multi-directional variable thickness thin plate with multiple materials. *Structural and Multidisciplinary Optimization*, **59**, (5), (2019), pp. 1503–1520. https://doi.org/10.1007/s00158-018-2143-8.